Journal of Civil Structural Health Monitoring (2023) 13:1483–1497
https://doi.org/10.1007/s13349-022-00623-y

ORIGINAL PAPER

Water–structure interaction analysis of a segmental bridge using ambient vibration testing at different water levels

Wilson Hernandez[1] · **Alvaro Viviescas**[2] · **Carlos Alberto Riveros-Jerez**[3]

Received: 2 May 2022 / Accepted: 20 August 2022 / Published online: 6 September 2022

Abstract

Updating a finite-element (FE) model using dynamic parameters obtained from field testing requires an adequate understanding of the variation of such parameters due to changes in environmental conditions. This paper presents an experimental program to study the influence of the water–structure interaction in the dynamic response of a prestressed concrete segmental bridge with partially submerged piers in an artificial reservoir. The bridge, located in Colombia, has a total length of 558 m. Ambient Vibration Tests (AVTs) consisted of four experimental campaigns at different water levels to perform modal identification. In addition, existing empirical formulations accounted for the effect of the hydrodynamic masses concentrated in the piers. This paper shows that updating FE models from identified dynamic properties in partially submerged bridges involves percentage reductions in natural frequencies related to the reservoir's water level. Thus, providing a better insight into the incidence of water–structure interaction on partially submerged bridges' dynamic response. Finally, considerations during dynamic characterization tests are discussed.

Keywords Ambient vibration test · Model updating · Water–Structure interaction · Segmental bridge

Long-term bridge monitoring systems largely depend on parameters, such as the data acquisition system, data processing, and the bridge monitoring baseline (defined as the initial input to determine the variation of modal parameters). Therefore, the monitoring baseline consists of a set of indicators or parameters of interest obtained experimentally from an initial state of the monitoring phase. The most widely used parameters in bridge dynamic characterization are natural frequencies, mode shapes, and damping ratios. Correctly determining such parameters allows the model updating process to monitor and evaluate modal parameters in subsequent measurement campaigns. AVTs have been widely used to identify the dynamic properties of bridges at a relatively low operating cost. It is the most attractive aspect in selecting the excitation force compared to mechanical devices for forced excitation.

✉ Carlos Alberto Riveros-Jerez
carlos.riveros@udea.edu.co

[1] Research and Development University, Bucaramanga, Colombia

[2] Industrial University of Santander, Bucaramanga, Colombia

[3] University of Antioquia, Medellín, Colombia

The Unión viaduct with a box girder section of segmental typology built in Colombia was dynamically characterized by [1]. Model updating was conducted during different construction stages; therefore, different FE models were considered to represent the effect of the construction loads on the dynamic characterization of the bridge. Significant deviations in modal identification were associated with uncertainty in load determination, especially during the cantilever construction and the practical limitations to account for the effect of the travelling formworks in the mass used in the simulation. In addition [2], also showed significant deviations in the determination of the Optimum Sensor Placement (OSP) locations obtained from the Effective Independence (EI) [3] method by considering numerical and experimental derived mode shapes due to modelling uncertainties on the mass during the construction process. The Berta bridge built in Deep Valley, Turkey, was dynamically characterized by [4] using an updated FE model obtained from AVTs to consider the effect of the wind forces and anthropic loads on the response of the bridge. The model updating process was conducted by modifying the mechanical properties of the materials until the difference between the numerical and experimental frequencies was minimized. Investigations with a similar approach have also been presented by [5, 6].

At the beginning of the twenty-first century, China's economic growth led to the development of road connectivity dominated by the type of T-style rigid frame bridge or cantilever girder bridge with suspended girders. As a result, several studies have pointed out the necessity of using a limited number of sensors to conduct modal updating [7]. Developed an updated numerical model of a bridge on the No 312 National Highway across Jian Guang Railway. The bridge has spans of 40 m, and model updating was conducted using data collected from AVTs to adjust the mechanical properties of the materials in terms of specific weight and modulus of elasticity. On the other hand, The El Carrizo bridge, located on the Durango Mazatlán Mexico highway, with the central section defined as cable-stayed with a double cantilever structure of 70.6 m ending with Nebraska-type post-tensioned beams, was seriously affected by a fuel fire from a vehicle accident. A rehabilitation strategy was developed in three stages: repair of box girders, construction of temporary lanes and installation of existing transverse elements without removing the existing ones [8]. During the repair processes, the bridge was instrumented with strain gauges, fiber optic inclinometers, temperature sensors and linear variable differential transformer (LVDT) sensors that allowed model updating during each rehabilitation stage. The authors analyzed the dynamic response of a part of the bridge subjected to repair by employing a dynamic load test with the circulation of a 22 T vehicle at 50 km/h. The FE model was updated by adjusting the mechanical parameters of the materials in terms of element dimensions and modulus of elasticity. The authors concluded that one of the benefits of structural monitoring is to verify the integrity of the rehabilitation work to guarantee the users' safety. The above studies stress the necessity of an excellent symbiosis between field measurements and FE models that allows virtual representations to evaluate the structural state in real-time to complement decision-making strategies [9]. However, a large number of sensors will increase the monitoring system budget. Therefore, OSP is essential for reliable structural conditions in risk assessment and bridge management strategies [10].

In the modal identification process, the desired number of sensors and positions must be carefully determined so that the sensor configuration (number and position) allows the bridge mode shapes to be correctly identified [11]. Various approaches for identifying OSP locations can be found in [12]. Thus, the calibration process can be considered a critical stage in obtaining the bridge monitoring baseline, which provides essential information to detect any anomalous bridge behaviour in the long term [13]. Several methods for model updating have recently been developed, including sensitivity analyzes and optimization algorithms [14]. Although environmental parameters such as temperature, relative humidity, and the water level may not be relevant in the FE model updating process, they are decisive in some cases. For example, in 1997, [15] presented a study on the dynamic characterization of the Alamosa Canyon bridge using forced vibration with data recording periods of 2 h during one full day of testing (24 h), variations of up to 5% in identification of modal parameters were reported, mainly associated with temperature gradients. In the case of bridges with partially submerged piers, the dynamic response is actively influenced by the coupling of masses between the surrounding water and the bridge, which affects the dynamic properties as a function of the water level.

To provide a better understanding of the effects of the water level (partially submerged long-span segmental bridges) in determining modal parameters, several analytical and numerical approaches have been recently proposed, which can be classified into three different categories as stated by [16]: (i) added mass formulations in which the effect of the water–structure interaction is approximated by an added mass, (ii) solutions based on continuum mechanics that use the wave equation to include the effect of hydrodynamic pressure, and (iii) numerical solutions that use finite or boundary elements to model the effect of the surrounding water. In the present work, to model the effect of the surrounding water in partially submerged bridges, the added mass approach (using five empirical and semi-empirical equations) is adopted to update the FE model developed for a case study of a segmental bridge using data collected from AVTs conducted for four levels of water in the reservoir.

1 Numerical simulation of mass equations

Five semi-empirical equations are selected herein for model updating. Equation (1) is proposed in this paper in analogy to the effect of hydrostatic pressure. Equation (2) is recommended by the Colombian bridge code—LRFD—CCP14 as a function of the flow rate of the water current [17]. Equation (3) was developed in 1965 by Goto and Toki for rectangular profile columns. Equation (4) was developed by [18] as a simplified expression of hydrodynamic pressure acting on circular columns. The accuracy of the formula was verified by theoretical analysis, comparison with equations developed by [19] and Goto and Toki [20] and numerical models based on the potential-based fluid-element method (PBFEM). Equation (4) was developed for column heights ranging between 20 and 150 m and diameter–height ratios from 0.05 to 1. Ref. [18] highlighted that Eq. (4) fits cylindrical columns better than the equation developed by Goto and Toki, which underestimates the hydrodynamic effects when the diameter–depth ratio is less than 0.5. Finally, Eq. (5) was developed by [21] and [22] and focused on rectangular columns. It considers the effect of hydrodynamic pressure on two dominant variables: the column's submerged height and the cross-sectional dimensions. Validation of Eq. (5) was conducted in a 6-span box girder

bridge, but during such validation, it was found that the effect of soil–structure interaction was dominant over hydrodynamic pressure due to the presence of soft soils [21].

In Eq. (1), H_p is the submerged heigh, B_p is the perpendicular dimension, β is the reduction factor [kN/m^{2}g]. In Eq. (2), C_D is the drag coefficient for the cross-sectional geometry, w is the specific weight of water $[\mathrm{N/m^3}]$, v is the water velocity [m/s], and A is the cross-sectional area. In Eq. (3), W_0 is the density of the water, A_0 is the cross-sectional area of the column, h is the height of the submerged column, a, b are, respectively, the perpendicular and parallel dimensions of the column, y is the variation of submerged height. In Eq. (4), h is a function of the submerged height of the column, ρ is the density of the water, a is the equivalent area radius for a rectangular section, and z is the delta height. In Eq. (5), a, b are the cross-sectional dimensions of the column, where a is the side perpendicular to the direction of water movement, ρ is the density of the water, h is the height of the submerged column, d_1, d_2 are two adjustment coefficients, and y is the height measured from the depth of the water level:

$$m_{\mathrm{add}} = \beta H_p B_p \left(\frac{\mathrm{kN}}{\mathrm{g}}\right) \tag{1}$$

$$m_{\mathrm{add}} = \frac{\left(C_D \frac{w}{2g} V^2\right) \cdot A}{g} \left(\frac{\mathrm{N}}{\mathrm{g}}\right) \tag{2}$$

$$m_{\mathrm{add}} = \frac{W_0 A_0 b}{ga}\left(1 - \frac{b}{4h}\right)\sqrt[3]{\frac{y}{h}}\left(\frac{\mathrm{kg}}{\mathrm{g}}\right) \tag{3}$$

$$m_{\mathrm{add}} = \rho\pi a^2\left[\frac{h^{1.5}}{(0.1a^2 + 1.9a - 1.7) + h^{1.5}} \cdot \left(1 - \mathrm{e}^{\left[\frac{2a+h}{ah}(z_i - h)\right]}\right)\right]\left(\frac{\mathrm{kg}}{\mathrm{g}}\right) \tag{4}$$

$$m_{\mathrm{add}} = 4\rho a^2 d_1\left[1 - \frac{y}{h}\mathrm{e}^{d_2(y/h-1)}\right] \cdot \left(\frac{\mathrm{kg}}{\mathrm{g}}\right)$$

$$d_1 = m_1\left(\frac{2a}{h}\right)^{m_2} + 0.412\left(\frac{a}{b}\right)^{-1.012} + 0.952$$

$$d_2 = n_1\left(\frac{2a}{h}\right)^{-1.26} + n_2$$

$$m_1 = -0.35\left(\frac{a}{b}\right)^{-1.092} - 0.198$$

$$m_2 = 0.766\mathrm{e}^{0.0471(a/b)} - 0.782\mathrm{e}^{-1.401(a/b)}$$

$$n_1 = -0.0157\left(\frac{a}{b}\right)^2 + 0.194\frac{a}{b} + 0.846$$

$$n_2 = 0.004\left(\frac{a}{b}\right)^2 - 0.0533\frac{a}{b} + 2.143 \tag{5}$$

2 Case study

The Tablazo bridge is a prestressed segmental box-girder bridge with a total length of 558 m. The heights of the piers are 57 m (south access), 109 m (mid-span) and 90 m (north access), and the bridge's width is 10.55 m. The bridge was built using 115 segments with a variable height ranging from 9 m in pier connection to 3 m in mid-span, as shown in Fig. 1. The compressive strength of the concrete for piers and deck is 35 MPa, and the steel strand of grade 270 low-relaxation conforming to ASTM A 416. The Tablazo bridge provides a road connection between the city of Bucaramanga—the capital city of the department of Santander—and the city of San Vicente de Chucurí and is part of the hydroelectric project of the Topocoro dam. The bridge piers are currently submerged to a variable level, leaving a minimum headroom of 28 m.

2.1 FE model of the bridge

The FE model of the bridge was assembled using the commercial software MIDAS CIVIL©. Each bridge segment was modelled following the dimensions and material properties specified in the construction drawings provided by the Government of Santander. The modulus of elasticity for concrete was 28,091 MPa for concrete of 35 MPa, assuming a linear behaviour of the material. The initial FE model was made up of 240 beam elements, and after refining the mesh, the final FE model consisted of 1340 beam elements. Fixed boundary conditions were assigned to the FE model without the soil–structure interaction effect, since the bridge is supported on firm soil according to the results of soil exploration reports. Therefore, fixed support is considered as the modelling support condition with displacement restrictions in Y (transverse), Z (vertical), rotation in Rx (longitudinal) and Rz in the access supports. The steel strand grade 270 low-relaxation conforming to ASTM A 416 was included in groups of 12 and 19 cables using factors for friction and curvature losses of μ = 0.20 and K = 0.0016/m. Figure 2 shows the mode shapes 1-Y, 1-Rz and 1-Z obtained from the FE model.

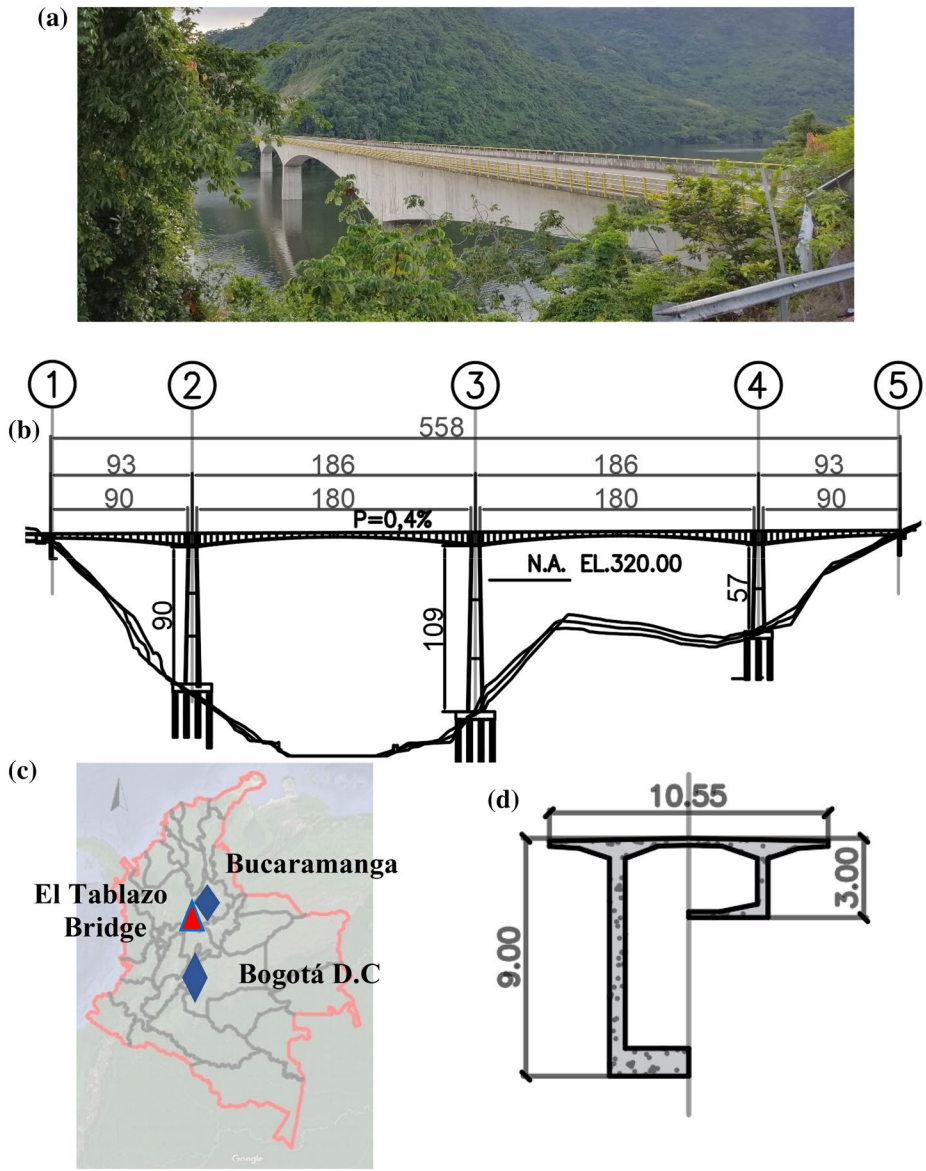

Fig. 1 Tablazo bridge. **a** View from the south access. **b** Side view (unit: m). **c** Location of the bridge **d** Cross-sections (unit: m)

2.2 Ambient vibration testing

Two Kinemetrics© Obsidian® reference high sensitivity balanced force triaxial accelerometers recorded and stored acceleration signals. The accelerometers have a dynamic range of 15 5Db in bandwidth up to 200 Hz, with a full-scale range between ± 2 to ± 4 g that synchronizes the data collection through a GPS antenna, as shown in Fig. 3. The water level was determined during 4 days of testing by measuring the distance from the water level to the bottom of the bridge deck. In addition, the temperature was recorded during periods of 1 h. On the other hand, a movement of the water in the bridge's transverse direction was identified with approximately equal velocities in the central area of the bridge and lower velocities in the vicinities of the reservoir shores. Although no water velocity measurements were made, a relevant effect of hydrodynamic mass in the longitudinal and transverse directions of the bridge is expected. Four AVTs were carried out on different days. In two AVTs, accelerations were recorded at 30 points spaced every 18 m, with time records every 20 min and a sampling frequency of 200 Hz. In the other two AVTs, accelerations were recorded at 18 points spaced every 30 m, with time records every 30 min and a sampling frequency of 200 Hz. The accelerometers were located in the partitions of the deck cross section to reduce the influence of local mode shapes (Fig. 4).

In Fig. 5, the green and red circles correspond to the nodes instrumented every 18 and 30 m, respectively. The black triangle corresponds to the location of the reference sensor (located at *L*/3 of the total length of the bridge measured from the north access). To minimize the influence of the number of sensors used in the AVTs, the mode shapes

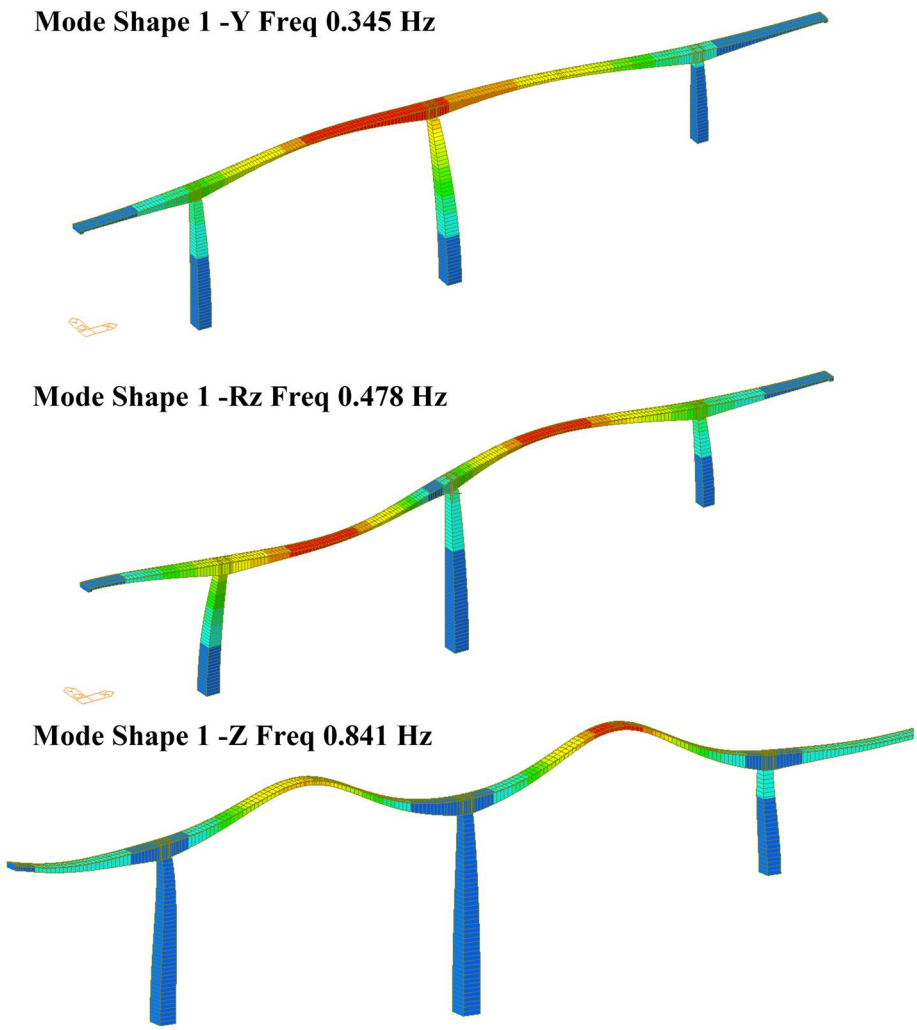

Fig. 2 Numerical mode shapes 1-Y, 1-Rz and 1-Z

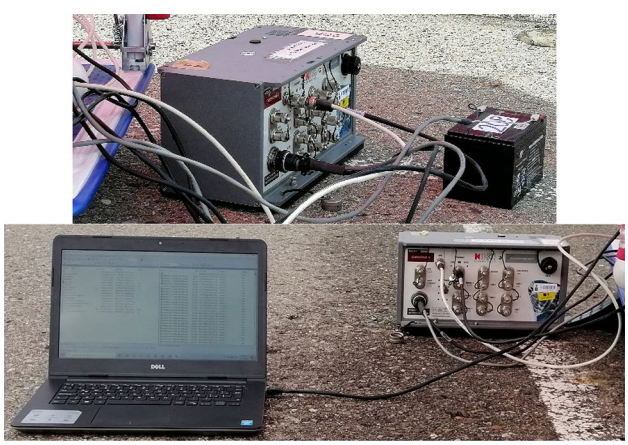

Fig. 3 Data acquisition system used in the AVTs

identified in AVTs 1 and 2 are selected to perform an OSP analysis using the Effective Independence (EI) method [23, 24]. The blue rectangles correspond to OSP positions. As a result, AVTs 3 and 4 (Fig. 5c, d) consist of a hybrid instrumentation mesh (combination of conventional separation + OSP locations). It is important to note that AVTs were conducted without interrupting traffic, and the number and type of vehicles were recorded at intervals of 1 h, as shown in Table 1. It is not expected that the passage of vehicles during field experiments has a significant effect in the dynamic response of the bridge. Despite the traffic differences (Table 1), the modal identification results presented in Table 1 are consistent. The temperature records collected during the execution of the AVTs ranged between 29 and 33 °C. The average temperature was 31.2 °C (deviation of 4.6 °C), as shown in Fig. 6. Due to the movement of the water in the reservoir as previously mentioned, it is expected that the effect of the hydrodynamic mass is more dominant in *X* and *Y* directions. Therefore, larger values of frequencies with respect to the ones obtained from the FE model are dominant in *Z* direction, where the bridge's weight is acting and imprecisions in bridge's weight determination have a relevant influence. On the other hand, the mode shape 1-RY

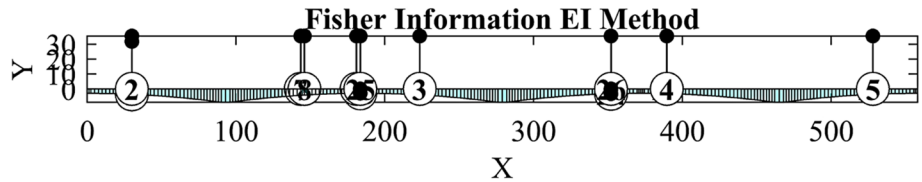

Fig. 4 OSP locations obtained from AVT 1

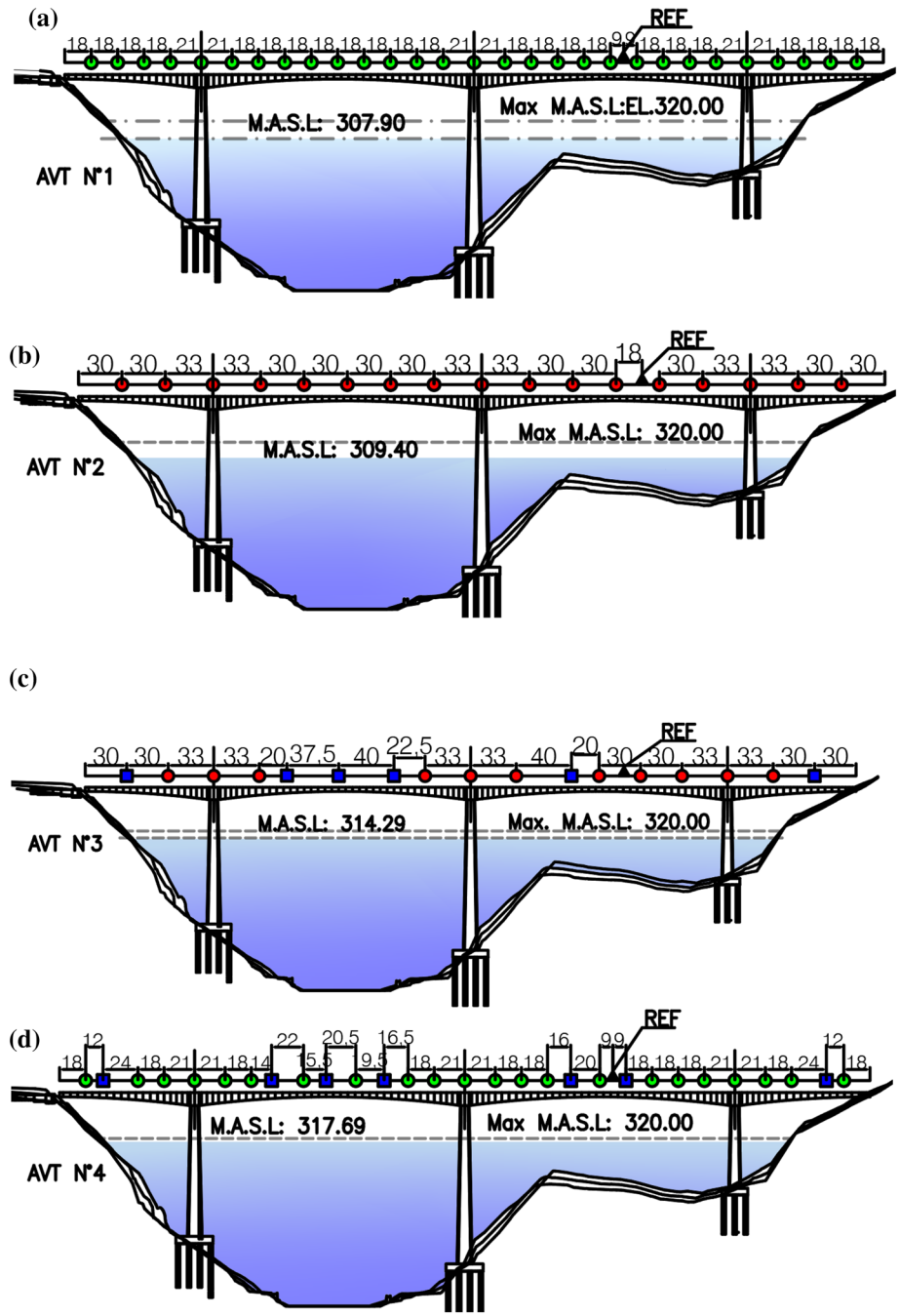

Fig. 5 Location of sensors in the AVTs

shows the same tendency and having a lager value of mass participation becomes more relevant. In this case, the water current is acting in one direction with lower velocities near reservoir shores and, therefore, does not affect significantly this rotational mode shape.

The identification of the dynamic parameters of the bridge (natural frequencies, mode shapes and damping

Table 1 Traffic density during the AVTs

Types of vehicles	AVT 1	AVT 2	AVT 3	AVT 4	Mean	SD
Passenger cars (1–2 T)	103	74	90	90	89	11.9
Two axle, four tire vehicles (2–3 T)	162	180	245	165	188	38.8
Buses (10–12 T)	17	23	21	23	21	2.8
Two axle, six tire vehicles (12–20 T)	78	123	77	110	95	23.1
Total	360	400	433	388		

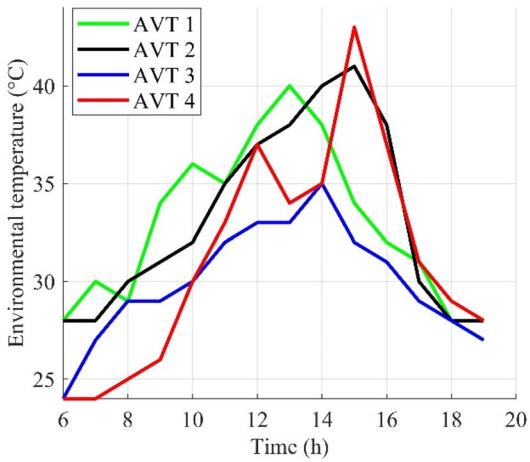

Fig. 6 Diurnal environmental temperature variation during the AVTs

ratios) was carried out using two techniques: the enhanced frequency domain decomposition (EFDD) technique [14] and the Stochastic Subspace Identification SSI technique [13]. In the ARTeMIS© software, the coordinates of the instrumented locations were assigned by entering in the nodes the acceleration records in the orthogonal direction (sampling frequency of 200 Hz). Finally, the power frequency spectra are obtained with corresponding mode shapes and damping ratios (EFDD, SSI techniques) for the frequency range between 0 and 5 Hz. Previously, a baseline adjustment was conducted, and the spectral density functions were calculated using Hanning windows of 1024 data (2^{10}) and considering the overlap between windows of 66%. For the EFDD technique, frequencies with a MAC rejection level greater than 0.9 were selected, and the damping ratios were calculated using the logarithmic decrement method. For the SSI technique, 100 eigenvalues were taken as the maximum dimension for the maximum frequency deviation, and a maximum variation coefficient of 0.1 in frequency and 5 in damping were selected. Finally, the computed values for the damping ratio range between 0.1% and 10%.

3 Results

Table 2 shows the 11 modal frequencies identified in the four AVTs, the frequency values obtained from the FE model, the percentage of mass participation and the estimated average modal consistency (MAC index) for each method. Table 3 shows the damping ratios estimated with the EFDD and SSI methods, with maximum values up to 3.3% identified with the SSI method. On the other hand, maximum values up to 2% are identified with the EFDD method. These results are consistent with those reported by [25]. The authors conducted modal identification using the EFDD and SSI in two concrete bridges, finding values of damping ratios of up to 2.5% and standard deviations of up to 46.5%. In a different study, [26] conducted modal identification using the EFDD and SSI in two frame structures. The authors found that the values of the damping ratios identified with SSI vary widely with respect to those identified with EFDD due to the method's sensitivity to the variation of the signal content for low frequencies. Finally, the instrumentation of a laboratory-scale dam allowed the identification of the dynamic properties using the EFDD and SSI methods before and after the filling of the reservoir at scale [27]. The authors identified decreases in frequency values in both methods and substantial increases of up to 8% in damping ratios with the SSI method. In addition, [28] reported that the time-series length affects the determination of damping ratios in the SSI method. Therefore, the AVT 2 and AVT 3 tests (recording times of 30 min) show damping ratios with an average standard deviation of 60%, which is lower than the value found in tests AVT1 and AVT4 (recording times of 20 min), as shown in Table 3. On the other hand, the MAC modal consistency presented in Table 2 is 8% higher for the EFDD method compared to values obtained with SSI. This trend is similar to that reported in [25]. When comparing the frequency values reported in Table 2, there were differences of up to 14% lower than the numerical values. Figures 7 and 8 show the power frequency spectrum of the 11 mode shapes and the mode shapes with the highest percentage of mass participation, respectively.

The inconsistencies of the FE model concerning the experimental data suggest the absence of a fundamental parameter in the initial FE model. The natural frequency is related to two critical parameters: the system's mass and

Table 2 Numerical and experimental modal frequencies

Mode	Mass part %	Frequency (Hz)									Mean MAC EFDD	Mean MAC SSI
		FEM	EFDD				SSI					
			AVT 1	AVT 2	AVT 3	AVT 4	AVT 1	AVT 2	AVT 3	AVT 4		
1-Y	47.4	0.35	0.32	0.32	0.31	0.31	0.36	0.36	0.34	0.38	0.94	0.81
1-RZ	33.0	0.48	0.44	0.44	0.44	0.43	0.46	0.47	0.45	0.45	0.97	0.74
2-Y	11.5	0.69	0.63	0.63	0.62	0.62	0.65	0.62	0.62	0.62	0.89	0.55
1-Z	12.5	0.84	0.86	0.82	0.82	0.81	0.81	0.81	0.82	0.82	0.67	0.86
3-Y	10.7	1.28	1.13	1.13	1.12	1.11	1.10	1.12	1.12	1.15	0.89	0.82
2-X	8.6	1.36	1.26	1.25	1.25	1.24	1.25	1.26	1.25	1.26	0.95	0.90
3-Z	7.4	1.49	1.50	1.48	1.48	1.49	1.50	1.49	1.50	1.53	0.83	0.73
1-RY	21.8	1.74	1.93	1.97	1.96	1.94	1.91	1.91	1.91	1.91	0.86	0.87
4-Z	3.3	1.94	2.00	2.02	2.02	2.01	2.03	2.04	2.03	2.03	0.96	0.97
3-X	2.8	3.03	2.92	2.92	2.91	2.90	2.92	2.92	2.91	2.91	0.78	0.78
2-Z	9.6	3.12	3.29	3.30	3.29	3.28	3.31	3.31	3.26	3.28	0.82	0.84

Table 3 Experimentally determined modal frequencies and damping ratios

Mode shape	AVT 1		AVT 2		AVT 3		AVT 4	
	EFDD	SSI	EFDD	SSI	EFDD	SSI	EFDD	SSI
1-Y	1.85	1.28	1.51	0.32	1.30	1.31	1.64	3.33
1-RZ	0.00	1.27	0.95	0.83	0.96	0.28	1.03	1.15
2-Y	0.00	0.91	0.80	0.72	0.85	0.93	0.00	0.84
1-Z	0.00	2.77	1.94	2.04	1.05	1.09	1.65	3.11
3-Y	0.89	0.78	0.77	0.74	0.97	1.12	0.93	3.31
2-X	0.74	0.87	0.68	0.63	0.68	0.61	0.71	0.24
3-Z	0.79	1.11	0.71	1.07	0.60	0.51	0.00	1.54
1-RY	1.22	0.81	1.09	0.67	1.05	0.71	1.11	0.68
4-Z	1.33	0.68	0.95	0.66	0.70	0.60	0.97	0.79
3-X	0.68	0.70	0.56	0.46	0.74	0.52	0.82	0.70
2-Z	0.71	0.60	0.70	0.91	0.72	0.64	0.65	0.64

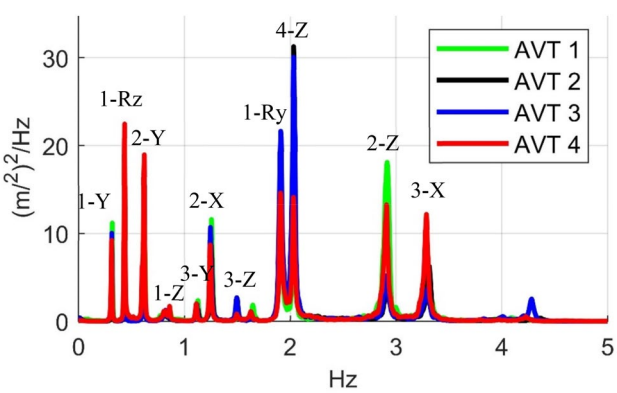

Fig. 7 Power spectrum for the AVTs (Units: $[m/s^2]^2/Hz$)

stiffness. According to the investigations reported by [29, 30], the decrease in the modal frequency values of structures submerged in water can be similar to hydrodynamic mass due to the effect of the water added to the system and given the relatively short commissioning time (5 years) of the bridge, no significant decreases in frequency attributed to loss of rigidity in the bridge are expected. Therefore, using Eqs. (1)–(5), hydrodynamic mass values are added to bridge piers using the water levels measured on the test days (as shown in Fig. 5). Equations (1) and (2) require a preliminary sensitivity analysis to identify the adjustment factor and water velocity value that achieve the highest MAC index. In some cases, estimating with adequate precision the dynamic response of the bridge under the effect of hydrodynamic forces is limited in the appropriate dynamic model approach to be used in the absence of validations in full-scale tests. Ref. [31] employed the concept of added mass to explain the decrease in experimental natural frequencies detected in a large-scale laboratory test, solving the fourth-order Runge–Kutta equation of motion to finally estimate the factor α, which is the ratio between

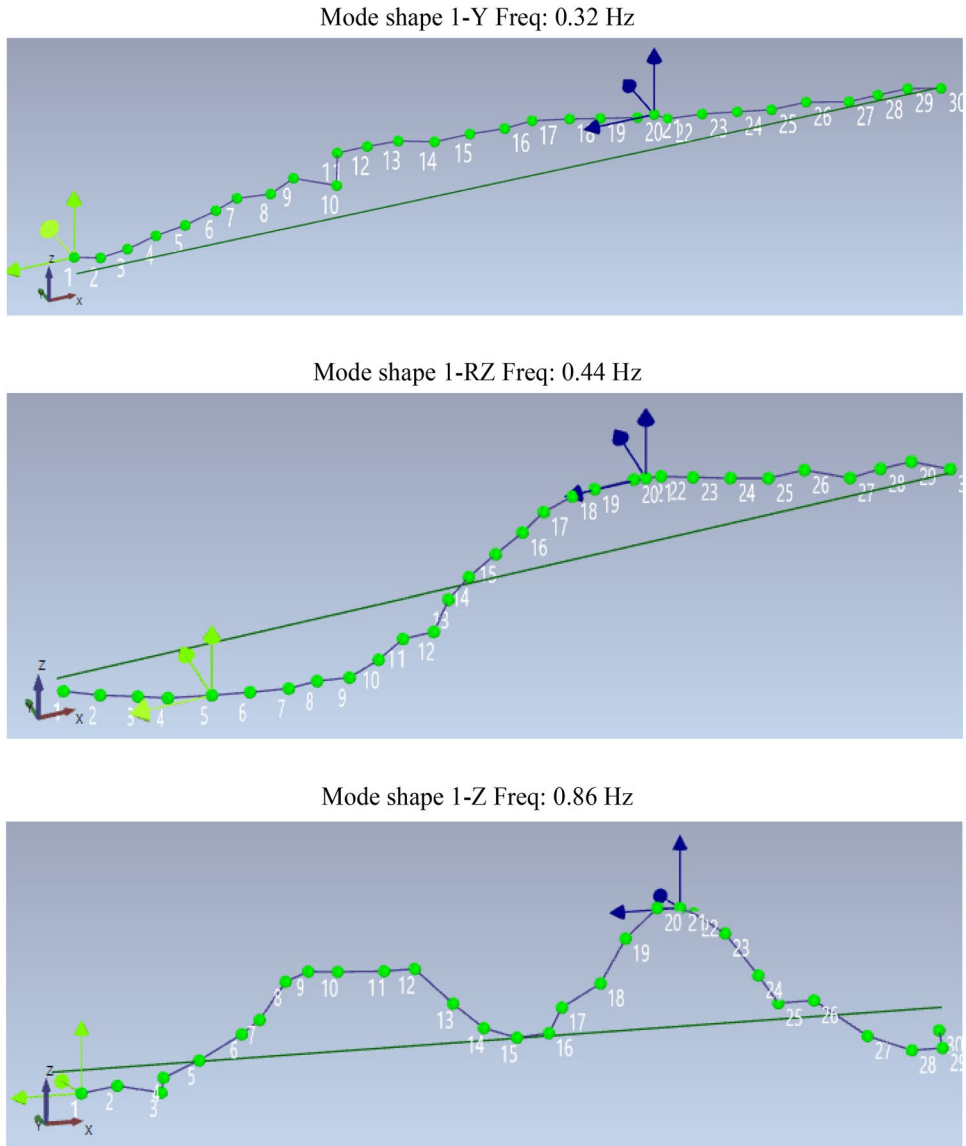

Fig. 8 Identified mode shapes using the EFDD technique (AVT 1)

the added m_{add} and the dry mass (measured in air) m_{dry} as shown in Eqs. (6) and (7):

$$\alpha = \left(f_a/f_w\right)^2 - 1 \tag{6}$$

$$m_{add} = m_{dry}\alpha \tag{7}$$

f_a, f_w correspond to the natural vibration frequencies of the bridge recorded in air and water, respectively. Ref. [31] reported two values of α for two water volume conditions. These values are 0.262 and 0.456. Currently, there is no consensus to determine the mass added to the system. Based on the values reported by [31], a sensitivity analysis is carried out with values of the estimated mass ranging from 10% to 100% (Eqs. 3, 4 and 5) to determine the factor α in all equations. Figures 9, 10, 11 and 12 show the MAC modal adjustment sensitivity analysis for AVT 1, 2, 3, and 4, respectively. Improvement in modal identification results of up to 3.25% is achieved in Eq. (5) with respect to the results provided by Eqs. (3) and (4). The final modal fit results of the factor α for the five equations are shown in Figs. 13, 14, 15, 16. It is possible to identify an ideal range for estimating the factor α (values between 0.3 and 0.5). This range of values is similar to the range reported by [31]. Equations (3), (4) and (5) show the best MAC modal fit results for $\alpha = 0.5$, 0.3 and 0.5, respectively. Equations (2) and (5) allow the best numerical modal fit based on the shape modes obtained from the AVTs. However, Eq. (2) has a practical limitation related to the field measurement of the water velocity and velocity variations. Table 4 shows the results of the comparison of frequencies obtained from the FE model and the AVTs. The average percentage error between the frequencies varies

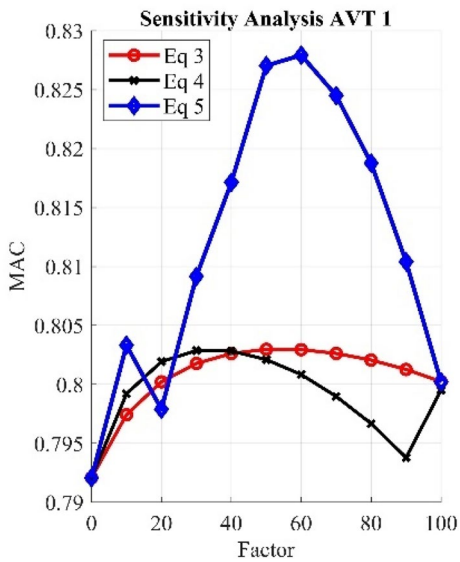

Fig. 9 Sensitivity analysis of factor α for AVT 1

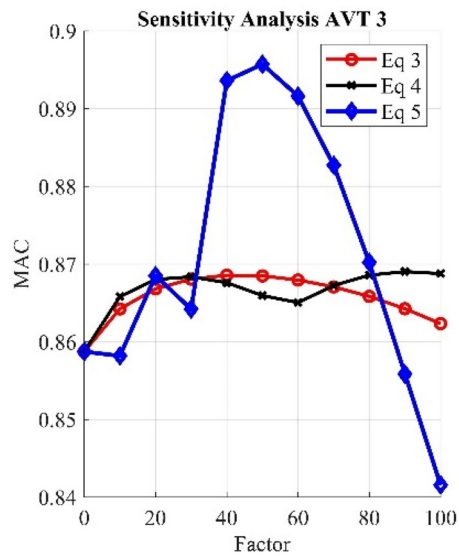

Fig. 11 Sensitivity analysis of factor α for AVT 3

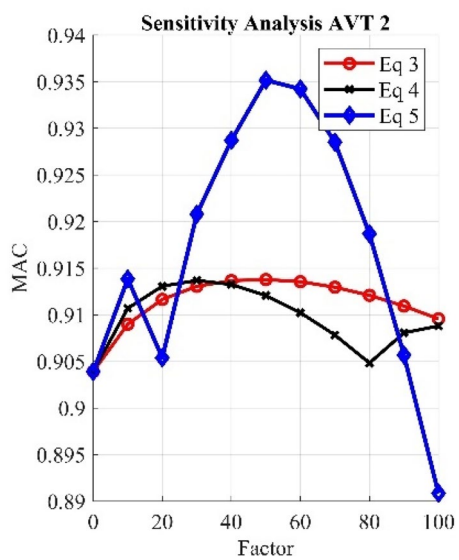

Fig. 10 Sensitivity analysis of factor α for AVT 2

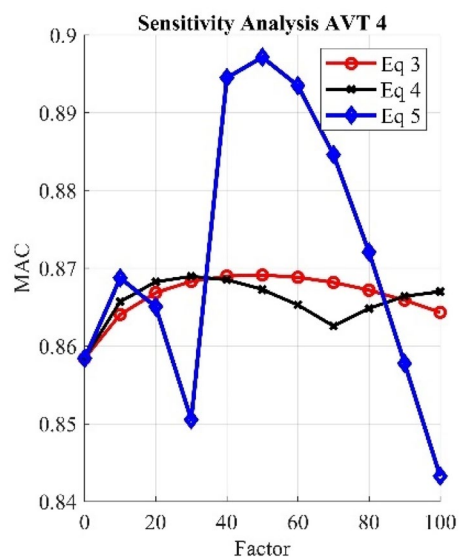

Fig. 12 Sensitivity analysis of factor α for AVT 4

between 3.6% and 0.76%. The best frequency adjustment is achieved in the mode shape 1-Y.

3.1 FE simulations

A set of numerical simulations was performed to analyze the incidence of the height of the water level (height of the submerged column) in the MAC modal adjustment for the four AVT tests. 100 numerical cases are selected and correspond to 10 water levels (variations from 10 to 100 m) and 10 added mass factors α from 0.1 to 1 (10–100% of added mass) based on Eq. (5). A schematic representation of the water levels is shown in Fig. 17, where the water level varies between 70 and 90 m. The eleven experimental AVT mode shapes are compared with the respective numerical mode shapes based on the average MAC index, as shown in Figs. 18, 19, 20, and 21. The highest modal fit is found between 60 and 90 m of water level with α factors that vary between 30% and 100%. It is important to note that as the corresponding water height in the AVT test is approached (AVT1: 74 m, AVT2: 76 m, AVT3: 81 m, AVT4: 83 m), the value of the factor α is reduced up to 30% (0.3). This effect

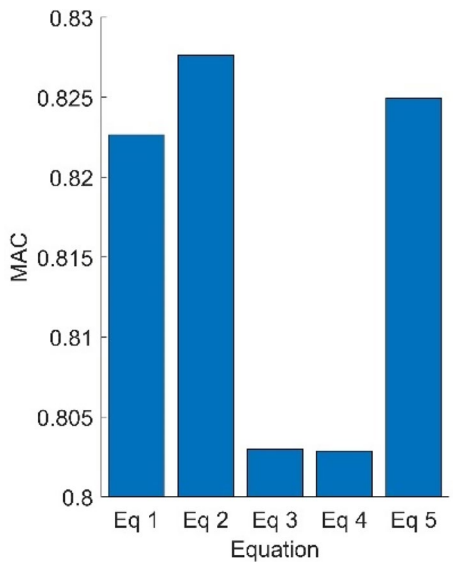

Fig. 13 Modal fit results of the factor α (AVT 1)

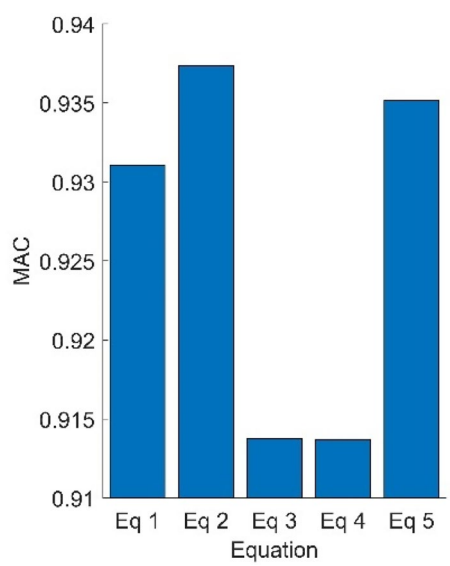

Fig. 14 Modal fit results of the factor α (AVT 2)

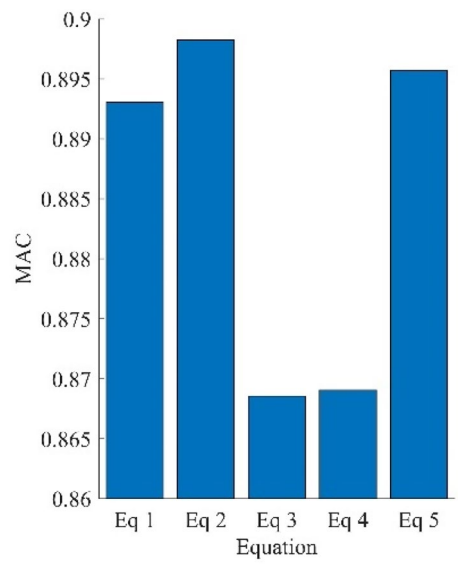

Fig. 15 Modal fit results of the factor α (AVT 3)

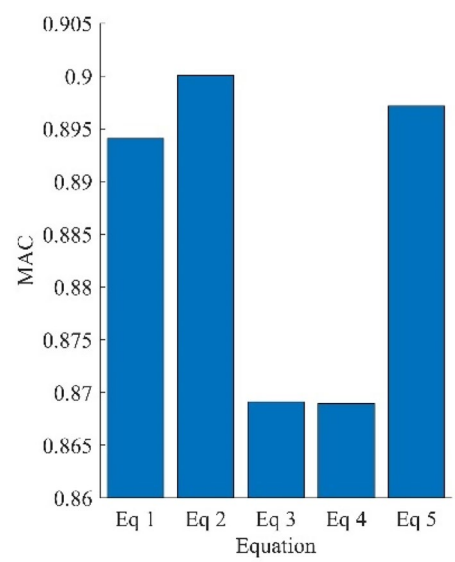

Fig. 16 Modal fit results of the factor α (AVT 4)

can be related to the total mass added to the columns, as shown in Fig. 22. Then, values of added mass between 2500 and 3500 T (mass of surrounding water in the columns) lead to the maximum MAC adjustment. Figures 18, 19, 20, 21 show the lowest values of MAC adjustment in blue and yellow color ranges related to mass values below 2500 T and above 3500 T, respectively.

4 Conclusions

This study presents a FE model updating process to consider the effect of fluid–structure interaction using data collected from field measurements. Assembling FE models from existing bridges requires field validation regarding material properties and element dimensions. However, in practical applications, field measurements are limited to some parameters, and the effect of fluid–structure interaction is relevant in partially submerged bridges. As a result,

Table 4 Frequencies obtained from the initial FE model, the updated FE model and the AVTs

Mode	FEM initial	AVT 1		AVT 2		AVT 3		AVT 4		% mean error initial	% mean error final
		EFDD	FEM	EFDD	FEM	EFDD	FEM	EFDD	FEM		
1-Y	0.35	0.32	0.32	0.32	0.32	0.31	0.32	0.31	0.32	9.9	1.9
1-RZ	0.48	0.44	0.46	0.44	0.46	0.44	0.45	0.43	0.45	9.7	4.5
2-Y	0.69	0.63	0.66	0.63	0.66	0.62	0.65	0.62	0.65	10	5.2
1-Z	0.84	0.86	0.82	0.82	0.82	0.82	0.82	0.81	0.82	1.7	−0.8
3-Y	1.28	1.13	1.24	1.13	1.24	1.12	1.22	1.11	1.2	14.4	9.4
2-X	1.36	1.26	1.3	1.25	1.29	1.25	1.26	1.24	1.24	9.2	1.9
3-Z	1.49	1.50	1.48	1.48	1.47	1.48	1.46	1.49	1.46	−0.2	−1.5
1-RY	1.74	1.93	1.88	1.97	1.86	1.96	1.84	1.94	1.83	−10.6	−5
4-Z	1.94	2.00	1.94	2.02	1.94	2.02	1.94	2.01	1.94	−3.4	−3.5
3-X	3.03	2.92	2.84	2.92	2.83	2.91	2.82	2.90	2.82	4.1	−2.9
2-Z	3.12	3.29	3.29	3.30	3.27	3.29	3.24	3.28	3.23	−5.2	−0.9

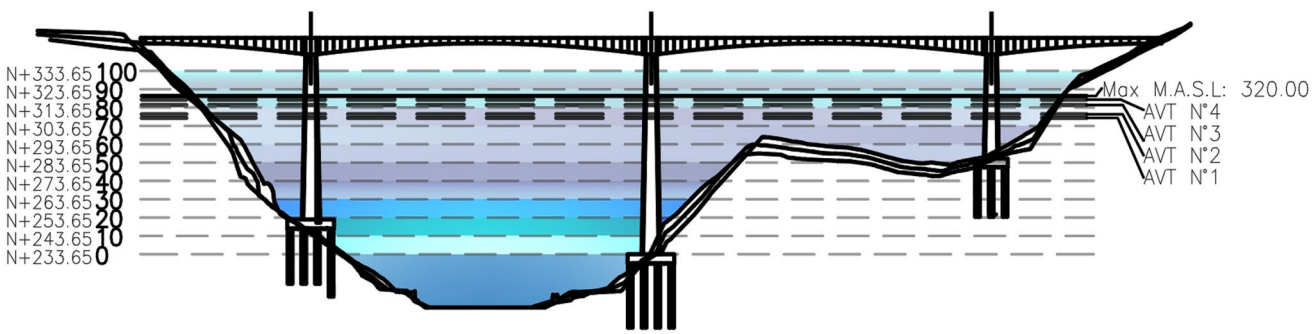

Fig. 17 Numerical simulations with different water level conditions

randomly modifying the modulus of elasticity of concrete without field testing validation in partially submerged bridges only increases uncertainties in the FE model updating process. Therefore, in this paper, four AVTs are conducted to consider the influence of the water level on the bridge's dynamic response. The model updating process presented in this paper improves the consistency of the numerical mode shapes by considering hydrodynamic masses concentrated in the piers. Another critical factor is related to the adequate planning of field measurements to consider the limited number of available sensors. This study conducted OSP analysis based on experimental mode shapes to overcome the inherent limitation of FE models in approximating the bridge's dynamic response. Therefore, two AVTs were conducted using OSP locations obtained from field testing, thus improving the quality of the FE updating process. The performance of five existing empirical formulations to consider fluid–structure interaction was studied during the FE model updating process. Based on comparisons between numerical and experimental mode shapes, the results show a better performance of Eq. (2), which indirectly considers the geometry through the drag coefficient. However, Eq. (2), presents limitations in practical applications regarding the difficulties of measuring the water velocity and the water velocity variations. Based on this consideration, the use of Eq. (5) is recommended in rectangular columns, typical of the type of bridge presented in this article. The analysis of the variation of the MAC modal fit with respect to the surrounding water level and the added mass factor obtained through numerical simulations allowed the determination of a relationship between the submerged column height and the added water mass that represents the fluid–structure interaction. The highest adjustment of the MAC index is obtained for water levels close to those recorded in the AVT tests and mass values between 2500 and 3500 T. The values of the added mass factor vary between 0.2 and 0.5, as identified by fitting the numerical models using the added mass approach to experimental values. With respect to the natural frequency in the air (before the reservoir is filled), variations of frequencies between 14% and 22%

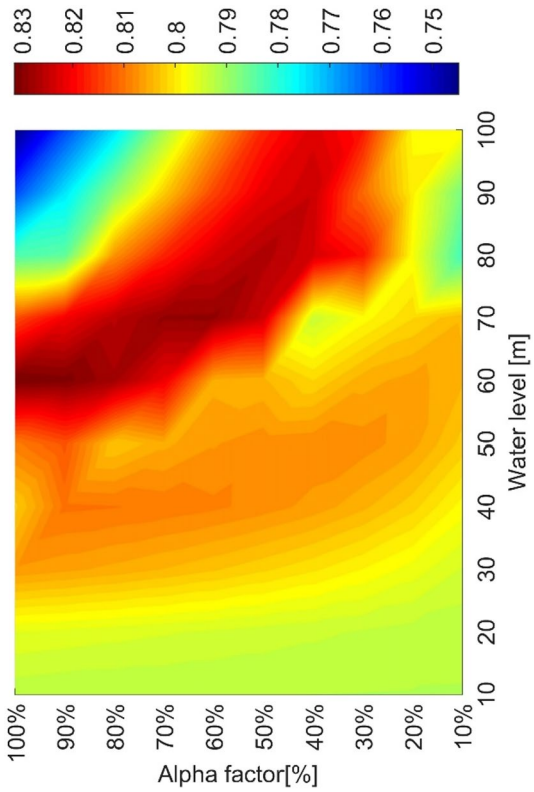

Fig. 18 MAC index AVT 1

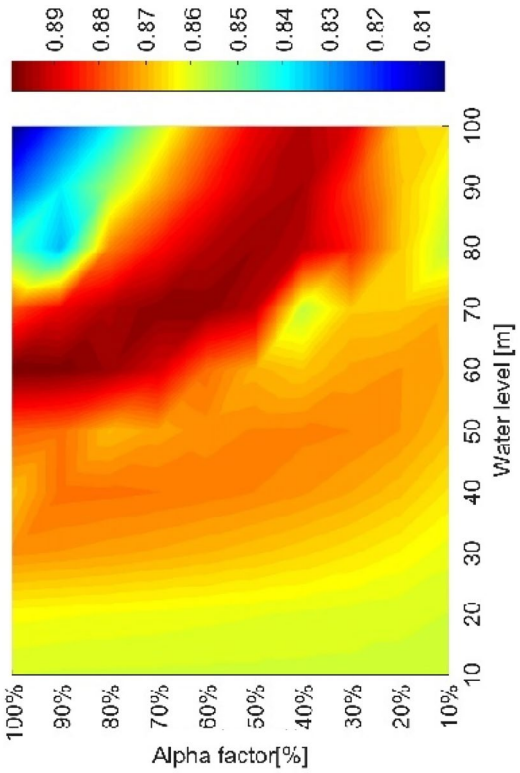

Fig. 20 MAC index AVT 3

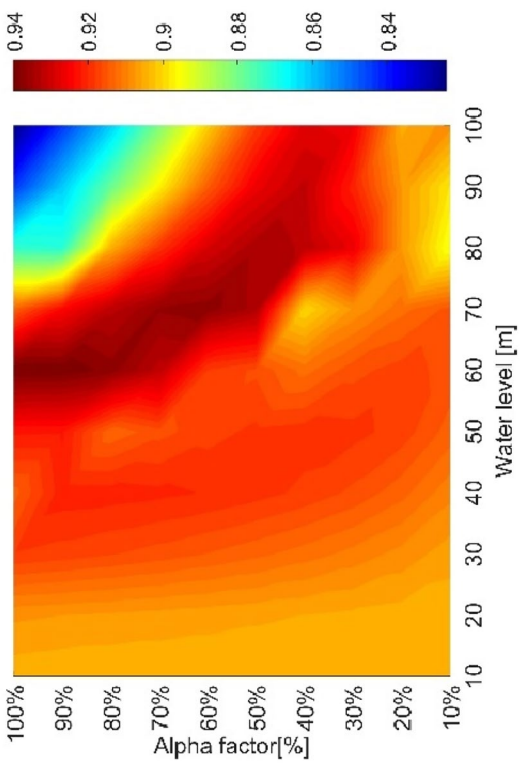

Fig. 19 MAC index AVT 2

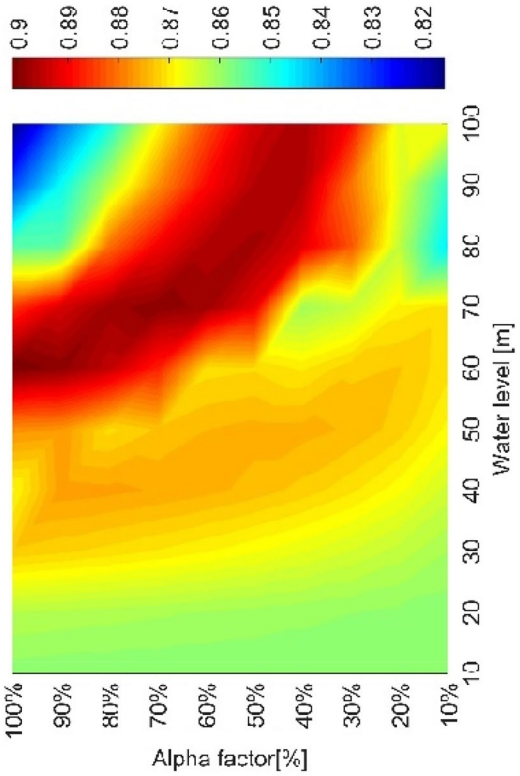

Fig. 21 MAC index AVT 4

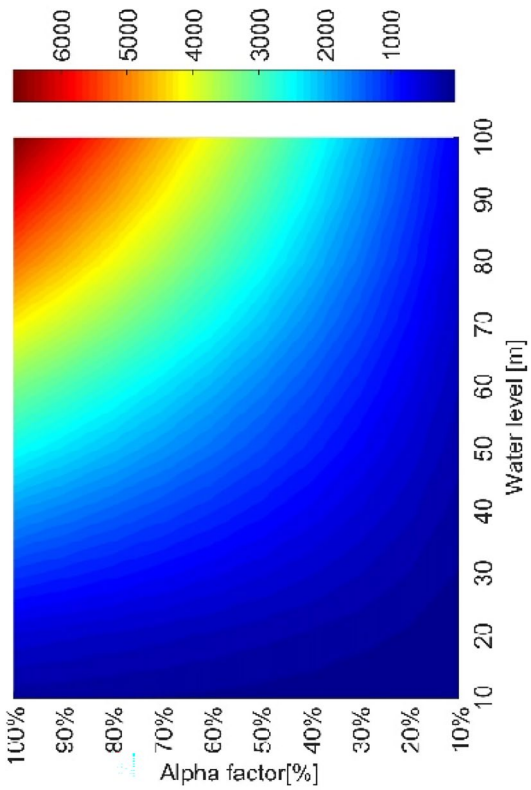

Fig. 22 Total mass added to the columns [T]

can be expected. This aspect highlights the importance of considering fluid–structure interaction in the dynamic characterization of partially submerged bridges.

Acknowledgements The authors greatly acknowledge the financial support provided by Minciencias through the project entitled "Monitoreo del comportamiento a largo plazo de la respuesta estructural de puentes viga cajón segmentales" (Project No. 82321) and the collaboration and information provided by the Government of Santander.

Funding Open Access funding provided by Colombia Consortium.

References

1. Hernandez W, Viviescas A, Riveros Jerez CA (2020) Verifying of the finite element model of the bridge on the vibration monitoring at different stages of construction. Arch Civ Eng LV(1)
2. Riveros Jerez CA, Viviescas Jaimes A, Chio G, Begambre Carrillo OJ, Hernandez W (2020) Optimal sensor placement of a box girder bridge using mode shapes obtained from numerical analysis and field testing. Rev EIA 17(34):1–12
3. Kammer DC (1991) Sensor placement for on orbit modal identification and correlation of large space structures. J Guid Control Dyn 14(2):251–259. https://doi.org/10.2514/3.20635
4. Kudu FN, Bayraktar A, Bakir PG, Turker T, Altunisik AC (2014) Ambient vibration testing of Berta highway bridge with post-tension tendons. Steel Compos Struct 16(1):21–44. https://doi.org/10.12989/scs.2014.16.1.021
5. Tian Y, Zhang J, Xia Q, Li P (2017) Flexibility identification and deflection prediction of a three-span concrete box girder bridge using impacting test data. Eng Struct 146:158–169. https://doi.org/10.1016/j.engstruct.2017.05.039
6. Fiore A, Marano GC (2018) Serviceability performance analysis of concrete box girder bridges under traffic-induced vibrations by structural health monitoring: a case study. Int J Civ Eng 16(5):553–565. https://doi.org/10.1007/s40999-017-0161-3
7. Huang M, Guo W, Zhu H, Li L (2008) Dynamic test and finite element model updating of bridge structures based on ambient vibration. Front Archit Civ Eng China 2(2):139–144. https://doi.org/10.1007/s11709-008-0028-4
8. Quintana JA et al (2021) Monitoring and evaluation of a highway bridge during major rehabilitation. Lect Notes Civ Eng 156(August):271–287. https://doi.org/10.1007/978-3-030-74258-4_19
9. Testa G, Bilotta A, Chioccarelli E (2021) Optimal sensor placement for dynamic identification of a reinforced concrete bridge. In: Concrete structures: new trends for eco-effiency and performance, pp 1481–1490. ISBN 978-2-940643-08-0
10. Bigoni C, Zhang Z, Hesthaven JS (2020) Systematic sensor placement for structural anomaly detection in the absence of damaged states. Comput Methods Appl Mech Eng 371:113315. https://doi.org/10.1016/j.cma.2020.113315
11. Liu K, Yan RJ, Guedes Soares C (2018) Optimal sensor placement and assessment for modal identification. Ocean Eng 165(June):209–220. https://doi.org/10.1016/j.oceaneng.2018.07.034
12. Castro-Triguero R, Murugan S, Gallego R, Friswell MI (2013) Robustness of optimal sensor placement under parametric uncertainty. Mech Syst Signal Process 41(1–2):268–287. https://doi.org/10.1016/j.ymssp.2013.06.022
13. Cunha Á, Caetano E (2005) From input–output to output-only modal identification of civil engineering struct. In: Proc. 1st Int. Oper. Modal Anal. Conf. IOMAC 2005
14. Omenzetter P et al (2013) Forced and ambient vibration testing of full scale bridges. Aberdeen. https://doi.org/10.13140/2.1.1168.5448
15. Doebling SW, Farrar CR, Cornwell P (1997) Statistical comparison of impact and ambient testing results from the Alamosa Canyon Bridge. In: Proc. Int. Modal Anal. Conf. IMAC, vol 1, September 2015, pp 264–270
16. Deng Y, Guo Q, Xu L (2017) Experimental and numerical study on modal dynamic response of water-surrounded slender bridge pier with pile foundation. Shock Vib 2017(ii):20–24. https://doi.org/10.1155/2017/4769637
17. Asociación Colombiana de Ingeniería Sísmica (2014) SECCION 3: Cargas y Factores de Carga. In: Norma Colombiana

de Diseño de Puentes, CCP 14, 1st edn. Asociación Colombiana de Ingeniería Sísmica, Bogotá, p 140
18. Jiang H, Wang B, Bai X, Zeng C, Zhang H (2017) Simplified expression of hydrodynamic pressure on deepwater cylindrical bridge piers during earthquakes. J Bridg Eng 22(6):04017014. https://doi.org/10.1061/(asce)be.1943-5592.0001032
19. Morison JR, Johnson JW, Schaaf SA (1950) The force exerted by surface waves on piles. J Pet Technol 2(05):149–154. https://doi.org/10.2118/950149-g
20. Goto H, Toki K (1965) Vibration characteristics and aseismic design of submerged bridge piers. In: Proc 3rd World Conf Earthquake Eng, pp 107–125. Available https://ci.nii.ac.jp/naid/10016215394/
21. Guo J, Wang K, Liu H, Zhang N (2021) Influence of water–structure and soil–structure interaction on seismic performance of sea-crossing continuous girder bridge. Adv Civ Eng. https://doi.org/10.1155/2021/7215289
22. Wang P, Zhao M, Du X (2019) Simplified formula for earthquake-induced hydrodynamic pressure on round-ended and rectangular cylinders surrounded by water. J Eng Mech 145(2):04018137. https://doi.org/10.1061/(asce)em.1943-7889.0001567
23. Castro-Triguero R, Garcia-Macias E, Flores ES, Friswell MI, Gallego R (2017) Multi-scale model updating of a timber footbridge using experimental vibration data. Eng Comput (Swansea, Wales) 34(3):754–780. https://doi.org/10.1108/EC-09-2015-0284
24. Farrar C, Todd M, Flynn E, Harvey D (2010) SHMTools Software. Los Alamos National Laboratory, New Mexico, p 199 [Online]. Available https://www.lanl.gov/projects/national-security-education-center/engineering/software/shm-data-sets-and-software.php
25. Magalhães F, Cunha Á, Caetano E, Brincker R (2010) Damping estimation using free decays and ambient vibration tests. Mech Syst Signal Process 24(5):1274–1290. https://doi.org/10.1016/j.ymssp.2009.02.011
26. Stengel D (2009) System identification for 4 types of structures in Istanbul by frequency domain decomposition and stochastic subspace identification methods. University of Karlsruhe, Germany
27. Sevim B, Bayraktar A, Altunişik AC, Adanur S, Akköse M (2010) Modal parameter identification of a prototype arch dam using enhanced frequency domain decomposition and stochastic subspace identification techniques. J Test Eval 38(5):102731. https://doi.org/10.1520/jte102731
28. Jacobsen NJ, Andersen P, Brincker R (2006) Using enhanced frequency domain decomposition as a robust technique to harmonic excitation in operational modal analysis. In: Proc. ISMA2006 Int. Conf. Noise Vib. Eng., vol 6, pp 3129–3140
29. Liaw C-Y, Chopra AK (1974) Dynamics of towers surrounded by water. Earthq Eng Struct Dyn 3(1):33–49. https://doi.org/10.1002/eqe.4290030104
30. Sun GS, Liu CG (2014) Research on hydrodynamic pressure of deep water bridge structure. In: Int. Efforts Lifeline Earthq. Eng.—Proc. 6th China–Japan–US Trilateral Symp. Lifeline Earthq. Eng., 2008, 465–472. https://doi.org/10.1061/9780784413234.060
31. Schumacher T, Hameed AW, Higgins C, Erickson B (2021) Characterization of hydrodynamic properties from free vibration tests of a large-scale bridge model. J Fluids Struct 106:103368. https://doi.org/10.1016/j.jfluidstructs.2021.103368